

Computing the laser beam path in Optical Cavities:

A Geometric Newton's Method Based Approach

Davide Cuccato · Alessandro Saccon ·

Antonello Ortolan · Alessandro Beghi

Received:date / Accepted: date

Davide Cuccato, Corresponding author

Department of Information Engineering, University of Padova

Via Gradenigo, 6 35100 Padova, Italy

cuccatod@dei.unipd.it

Alessandro Saccon

Department of Mechanical Engineering (Dynamics and Control), University of Eindhoven

De Vielen 5612 AZ, Eindhoven, Netherland

saccon@tue.nl

Antonello Ortolan

INFN - National Laboratories of Legnaro

Viale dell'Università, 2 35020 Legnaro (PD), Italy

antonello.ortolan@lnl.infn.it

Alessandro Beghi

Department of Information Engineering, University of Padova

Via Gradenigo, 6 35100 Padova, Italy

beghi@dei.unipd.it

Abstract In the last decade, increasing attention has been drawn to high precision optical experiments, which push resolution and accuracy of the measured quantities beyond their current limits. This challenge requires to place optical elements (e.g. mirrors, lenses, etc.) and to steer light beams with sub-nanometer precision. Existing methods for beam direction computing in resonators, e.g. iterative ray tracing or generalized ray transfer matrices, are either computationally expensive or rely on overparametrized models of optical elements. By exploiting Fermat's principle, we develop a novel method to compute the steady-state beam configurations in resonant optical cavities formed by spherical mirrors, as a function of mirror positions and curvature radii. The proposed procedure is based on the geometric Newton method on matrix manifold, a tool with second order convergence rate that relies on a second order model of the cavity optical length. As we avoid coordinates to parametrize the beam position on mirror surfaces, the computation of the second order model does not involve the second derivatives of the parametrization. With the help of numerical tests, we show that the convergence properties of our procedure hold for non-planar polygonal cavities, and we assess the effectiveness of the geometric Newton method in determining their configurations with high degree of accuracy and negligible computational effort.

Keywords Geometric Newton method · Oblique manifold · Ring laser · Optical cavity

Mathematics Subject Classification (2000) 58E50,49Q99

1 Introduction

In advanced optics applications, it is required to optimize the geometry of optical elements, in particular, when very high performance is sought for. One of such applications regards the design of resonant optical cavities that are essential elements of a wide range of devices and experiments, e.g. in laser physics, angular metrology, atomic clocks stabilization, etc. In this paper we focus on *ring laser gyroscopes*, which are devices used for measuring angular rotations with very high accuracy [1,2,3]. The core element of a ring laser is a three-dimensional resonant optical cavity, formed by $N > 2$ mirrors that are placed at the vertices of a polygon. In the cavity, the laser beam travels a closed optical path, defining a polygon of perimeter p and area \mathbf{a} [2]. In rotation sensing, \mathbf{a} and p are the most relevant geometric quantities, since their value and stability define the device performance in terms of sensitivity and accuracy.

Generally speaking, increasing the cavity dimensions (i.e. p and \mathbf{a}) results in measuring devices with higher sensitivity. In fact, the intrinsic noise limiting the sensitivity of a ring laser is the shot noise, and its magnitude turns out to be inversely proportional to p . However, the increase of dimensions negatively affects the ring laser long term stability, since changes of the environmental conditions (e.g. temperature and pressure drifts) during the measurement process induce geometry deformations which result in beam-jittering noise with magnitude almost proportional to p [1,4].

Even if a trade off can eventually be made between the intrinsic and beam-jittering noises, to increase sensitivity and stability of an optical cavity, the latter noise must be reduced as much as possible. To this aim, different approaches can be taken, leading to monolithic or heterolithic designs of the optical cavity. In the monolithic approach, one exploits an ultra low expansion material (e.g. Zerodur or Invar) to form a “rigid frame” supporting the mirrors, thus achieving passive stabilization of the cavity geometry by regulating pressure and temperature of the environment. For instance, the four-meter-wide square cavity of “G” [4] (presently the most sensitive and stable ring laser for geodetic and seismic applications) has a monolithic design. In the heterolithic design, mirrors are fixed to a concrete or granite frame and equipped with handlers to react against changes in their relative positions, thus stiffening the geometry of the apparatus [5,6]. Geometry can also be optimized to reduce the cavity sensitivity to the beam-jittering noise, e.g. by adjusting the beams path to regular polygonal shapes [7,8]. The heterolithic design overcomes the limitations due to the maximum size of a machinable monolithic element, and it is therefore chosen for very high performance applications, such as fundamental physics [9], geodesy and geophysics [10]. Clearly, implementation of the active geometry control of a heterolithic optical cavity requires the identification of suitable signals, provided e.g. by some metrological precision system, proportional to mirror displacements, and the derivations of accurate models.

In this paper we derive a geometrical model of an heterolithic ring laser to efficiently calculate the beams configuration as a function of the mirror

positions and orientations. This problem has already been addressed in the literature. In particular, generalized ray transfer matrices analysis, based on the optical axis perturbation, has been used in [11], and in [12] iterative ray tracing methods are used. These approaches are based on overparametrized models of the ring laser mirrors or involve a large number of iterations. To overcome these limitations, we exploit the Fermat's principle and the geometric Newton's algorithm on matrix manifold. This tool has second order convergence rate and relies on a second order model of the objective function, that in the problem at hand is the cavity length p . In particular, the light path in a square cavity made of spherical mirrors is calculated, starting from the positions of their centers of curvature and the value of their curvature radii. As we avoid the use of coordinates to parametrize the beam position on mirror surfaces, the computation of the second order model does not involve the second derivatives of the parametrization. We show that the convergence properties of our procedure hold for the optical cavities of interest. Finally, we assess the effectiveness of the geometric Newton method in determining their configurations with high degree of accuracy and negligible computational effort.

The paper is organized as follows. In Sect. 2 notations and definitions are given. Sect. 3 is devoted to the problem statement and formulation. In Sect. 4 we review the geometric Newton's Algorithm, which is then specialized in Sect. 5 to the Oblique Manifold. In Sect. 6 the application of the proposed

algorithm to the square ring laser cavity is presented, and in Sect. 7 some numerical results are presented. Conclusions are drawn in Sect. 8.

2 Notation and Definitions

In this paper we make use of the theory of finite dimensional smooth manifolds and covariant differentiation as presented in [13,14]. The symbols in Tab. 2 will be used throughout the paper.

Notation

\mathcal{E}	Euclidean space \mathcal{E} .
$\mathcal{M}, \mathcal{N} \subseteq \mathcal{E}$	Embedded Submanifolds $\mathcal{M}, \mathcal{N} \subseteq \mathcal{E}$.
$x \in \mathcal{M}$	Element x of the manifold \mathcal{M} .
$f : \mathcal{M} \rightarrow \mathbb{R}, \bar{f} : \mathcal{E} \rightarrow \mathbb{R}$	Real valued functions on \mathcal{M} and \mathcal{E} such that $\bar{f}(x) = f(x)$ for $x \in \mathcal{M}$.
$\mathfrak{F}(\mathcal{M})$	The set of smooth real valued functions on \mathcal{M} .
$\mathfrak{F}_x(\mathcal{M})$	The set of smooth real valued function defined near $x \in \mathcal{M}$.
$T_x \mathcal{M}$	The tangent space to \mathcal{M} at $x \in \mathcal{M}$.
$\xi_x \in T_x \mathcal{M}$	The tangent vector ξ_x to \mathcal{M} at x .
$\mathfrak{X}_x(\mathcal{M})$	The set of smooth vector fields on \mathcal{M} near x .
$\xi \in \mathfrak{X}_x(\mathcal{M})$	Smooth vector field $\xi : x \mapsto \xi_x$ on \mathcal{M} at x .
$DF : T_x \mathcal{M} \rightarrow T_{F(x)} \mathcal{N}$	The tangent map of $F : \mathcal{M} \rightarrow \mathcal{N}$ at x .
$\partial f(x) \in T_x \mathcal{E}$	Euclidean Gradient of $f : \mathcal{E} \rightarrow \mathbb{R}$.
$\partial^2 f(x) : T_x \mathcal{E} \rightarrow T_x \mathcal{E}$	Euclidean Hessian of f .
$\langle \cdot, \cdot \rangle_{\mathcal{M}} : T_x \mathcal{M} \times T_x \mathcal{M} \rightarrow \mathbb{R}$	Riemannian metric on \mathcal{M} .
$\nabla : T_x \mathcal{M} \times \mathfrak{X}_x(\mathcal{M}) \rightarrow \mathfrak{X}_x(\mathcal{M})$	Riemannian connection on $\mathcal{M} \subset \mathcal{E}$.
$\text{grad } f(x) \in T_x \mathcal{M}$	Riemannian Gradient of $f : \mathcal{M} \rightarrow \mathbb{R}$.
$\text{Hess } f(x) : T_x \mathcal{M} \rightarrow T_x \mathcal{M}$	Riemannian Hessian of f .
\mathbb{S}^2	Unit Sphere $\{\mathbf{x} \in \mathbb{R}^3, \mathbf{x}^T \mathbf{x} = 1\}$
\wedge	Canonical cross product between vectors of \mathbb{R}^3 .
\otimes	Kronecker product of two matrices,
$d : \mathbb{R}^{n \times n} \mapsto \mathbb{R}^{n \times n}$	$(d(A))_{ij} = \begin{cases} A_{ij} & i = j \\ 0 & i \neq j \end{cases}$

The Riemannian connection ∇ is determined by the condition

$$D \langle \xi_x, \chi_x \rangle_{\mathcal{M}} [\eta_x] = \langle (\nabla_{\eta_x} \xi)_x, \chi_x \rangle_{\mathcal{M}} + \langle \xi_x, (\nabla_{\eta_x} \chi)_x \rangle_{\mathcal{M}}, \quad (2.1)$$

where $x \in \mathcal{M}$, $\eta_x \in T_x \mathcal{M}$, and $\xi, \chi \in \mathfrak{X}_x(\mathcal{M})$, i.e. it is the unique connection that is compatible with the Riemannian metric $\langle \cdot, \cdot \rangle_{\mathcal{M}}$ of \mathcal{M} . Moreover, if $\mathcal{M} = \mathcal{E}$, we have that the covariant derivative associated to the Riemannian connection of the vector field ξ with respect to η_x is simply the directional derivative, i.e. $\nabla_{\eta_x} \xi = D\xi[\eta_x]$.

3 Problem Statement and formalization for a ring laser cavity

We consider an optical cavity formed by N spherical mirrors. By indicating with $\mathbf{z}_k \in \mathbb{R}^3$ the coordinates of the position of the light spot on the k -th mirror with respect to the ground frame, the cavity optical length can be computed as $p = \sum_{k=1}^N \|\mathbf{z}_k - \mathbf{z}_{k+1}\|$ and the enclosed vector area as $\mathbf{a} = \frac{1}{2} \sum_{k=1}^N \mathbf{z}_k \wedge \mathbf{z}_{k+1}$, where we define $\mathbf{z}_{N+1} := \mathbf{z}_1$. By applying the formalism of geometric optics, we can model the k -th spherical mirror M_k as a sphere of center $\mathbf{c}_k \in \mathbb{R}^3$ and curvature radius $r_k \in \mathbb{R}^+$. The position of the laser spot on the k -th mirror can be expressed as $\mathbf{z}_k = \mathbf{c}_k + r_k \mathbf{x}_k$, where $\mathbf{x}_k \in \mathbb{S}^2$, see Figure 3.1.

A *configuration* for the laser beams in the optical cavity is defined as the ordered set of points $\mathcal{X} = (\mathbf{x}_1, \dots, \mathbf{x}_N) \in \underbrace{\mathbb{S}^2 \times \dots \times \mathbb{S}^2}_{N \text{ times}}$, which describe the positions of laser light spots on each of the N mirrors. In addition, we define the matrix of centers $\mathcal{C} = (\mathbf{c}_1, \dots, \mathbf{c}_N)$ and the matrix of curvature radii $\mathcal{R} =$

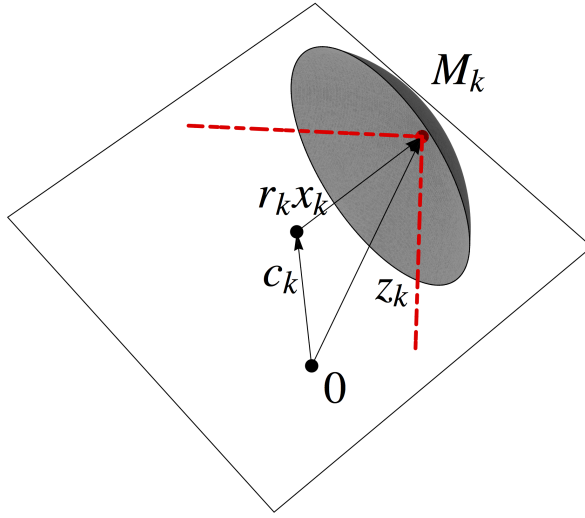


Fig. 3.1 Parametrization of the position of the laser spot on the k -th mirror M_k . With respect to the inertial frame origin O , the position of laser spot is $\mathbf{z}_k = r_k \mathbf{x}_k + \mathbf{c}_k$. The mirror M_k has radius r_k . Relative to the mirror center \mathbf{c}_k , the position of the laser spot can be parametrized as $r_k \mathbf{x}_k$, $\mathbf{x}_k \in \mathbb{S}^2$.

$\text{diag}(r_1, \dots, r_N)$. We refer to \mathcal{R} and \mathcal{C} as the *parameters* of the optical cavity. Given the cavity parameters \mathcal{R} and \mathcal{C} and a configuration \mathcal{X} , the corresponding laser beams path as well as the associated (scalar and vector) fields p and \mathbf{a} (see Section 1) can be computed.

Note that not every configuration \mathcal{X} is admissible as physical solution. In fact, the physical light paths have to be stationary points of p with respect to \mathcal{X} [15, Chap. 2]. This fact results out from the application of the Hamilton's principle to geometric optics, when we identify the Hamiltonian coordinates with the Euclidean coordinates of the laser spots and the action functional with the light optical path length. This result is known in optics as the Fermat's

principle, stating that the admissible paths are the ones that make their length stationary with respect to infinitesimal variations of the paths.

We turn now to the problem of computing the physical beam configuration given the cavity parameters \mathcal{R} and \mathcal{C} . To this end, we resort to an intrinsic geometric approach that avoids a local parametrization of the configuration manifold, only constraining the laser spots on each mirror to lie on the surface of a sphere. The advantages of this approach are to handle simpler expressions and to avoid the use of multidimensional spherical coordinates and derivatives of the parametrization.

The optical path length is a function of the cavity configuration \mathcal{X} and of the cavity parameters \mathcal{C} and \mathcal{R} . The configuration \mathcal{X} lives in the cartesian product of N unit spheres in \mathbb{R}^3 , $\underbrace{\mathbb{S}^2 \times \cdots \times \mathbb{S}^2}_{N \text{ times}}$. It is straightforward to show that this configuration manifold is an embedded submanifold of $\mathbb{R}^{3 \times N}$. This manifold is usually referred to as the Oblique Manifold of dimension $2 \times N$ [13]. The Oblique Manifold of dimension $n \times m$ is defined as

$$\mathcal{OB}(n, m) = \left\{ \mathcal{X} \in \mathbb{R}^{(n+1) \times m}, d(\mathcal{X}^T \mathcal{X}) = I_{m \times m} \right\} \cong \underbrace{\mathbb{S}^n \times \cdots \times \mathbb{S}^n}_m, \quad (3.1)$$

where the function d is defined in Tab. 2, and the tangent space at \mathcal{X} of $\mathcal{OB}(n, m)$ is

$$T_{\mathcal{X}} \mathcal{OB}(n, m) = \left\{ Y \in \mathbb{R}^{(n+1) \times m} : d(\mathcal{X}^T Y) = 0_{m \times m} \right\}. \quad (3.2)$$

It is worth mentioning that $\mathcal{OB}(n, m)$ inherits the (Riemannian) metric of $\mathbb{R}^{n \times m}$, i.e., we can define its Riemannian metric simply as $\langle \mathcal{X}, \mathcal{Y} \rangle_{\mathcal{OB}(n, m)} = \text{tr}(\mathcal{X}^T \mathcal{Y})$. Moreover, each column of \mathcal{X} in (3.2) is orthogonal to the corre-

sponding column of \mathcal{Y} , with respect to the (Riemannian) metric of \mathbb{R}^{n+1} , $\langle \mathbf{x}, \mathbf{y} \rangle_{\mathbb{R}^{n+1}} = \mathbf{x}^T \mathbf{y}$. In fact the columns of \mathcal{X} have the straightforward interpretation of points on \mathbb{S}^2 , so that each column of \mathcal{Y} represents a possible tangent vector to the corresponding column of \mathcal{X} , seen as a point of \mathbb{S}^2 .

A *physical configuration* $\hat{\mathcal{X}}$ is a cavity configuration that also satisfies Fermat's principle, such that it is a stationary point of the optical cavity length $p = p(\mathcal{X}; \mathcal{C}, \mathcal{R})$. Formally, the set of physical configurations is given by

$$\{\mathcal{X} \in \mathcal{OB}(2, N) : T_{\mathcal{X}}\mathcal{OB}(2, N) \ni \text{grad } p(\mathcal{X}; \mathcal{C}, \mathcal{R}) = 0\}. \quad (3.3)$$

By the Weierstrass theorem the set (3.3) can contain 2 or more elements being p a continuous function defined over a compact set $\mathcal{OB}(2, N)$. It is not possible, in general, to find closed form expressions for the elements of the set of physical configurations, therefore we resort to a numerical algorithm. We consider optical cavities with parameters \mathcal{C} and \mathcal{R} which slightly differ from the nominal values $\mathcal{C}^*, \mathcal{R}^*$. We assume also that the physical configuration \mathcal{X}^* of the optical cavity with parameters $\mathcal{C}^*, \mathcal{R}^*$ is known. Then, the physical configuration \mathcal{X}^* can be used as the initial condition for our algorithm. To efficiently compute a solution with desired accuracy, we propose to use a geometric Newton's method, which requires the computation of first and second order derivatives of the functions $p : \mathcal{OB}(2, N) \mapsto \mathbb{R}$. Such computation can be carried out in an elegant and efficient way by using advanced tools from differential geometry, involving the curvature and affine connection associated with the Riemannian manifold $\mathcal{OB}(2, N)$.

4 Review of the Geometric Newton's Method

We are interested in finding physical configurations of an optical cavity of length $p(\mathcal{X}; \mathcal{C}, \mathcal{R})$, with \mathcal{X} living in a Riemannian manifold. By the Fermat's principle \mathcal{X}^* can be found by solving Eq.(3.3). However, physical configurations \mathcal{X}^* are, in general, *inflections* and not extremal points of $p(\mathcal{X}; \mathcal{C}, \mathcal{R})$. Therefore we search for \mathcal{X}^* by minimizing the function $h = \|p(\mathcal{X}; \mathcal{C}, \mathcal{R})\|^2$. To this aim we resort to a geometric formulation of the Newton's method, by using a second order geometric model of p .

In the following we briefly review the Newton's algorithm formulation when used to find the zeroes of a real valued function h . Note that if $h = \|\text{grad } f\|^2$ then finding the zeroes of h is equivalent to find the stationary points of f . The classical formulation of the Newton's algorithm involves the computation of the Euclidean gradient $\partial h(\mathbf{x})$ and the inverse of the Euclidean Hessian $\partial^2 h(\mathbf{x})$. One could apply the Newton's algorithm to find the local minima of h , at the cost of computing third order derivatives of the function f . However, as shown in [13], the second order convergence rate is also achieved if at each iteration the function h is minimized along suitable directions, computed by means of the gradient and Hessian of f .

The extensions of the Newton algorithm to find stationary points of functions defined on an embedded submanifold of \mathbb{R}^n has been extensively studied in the literature [16, 17, 18, 19, 20]. We follow here the approach of Absil and others [13, 21, 22], who outlined an intrinsic formulation of the Newton algorithm when applied to optimization problems on embedded submanifolds.

Given a smooth manifold \mathcal{M} and a real valued function $f \in \mathfrak{F}(\mathcal{M})$ defined on \mathcal{M} , we build at each iterate $x_k \in \mathcal{M}$ a quadratic model \tilde{f} for f , along the direction η [13, Ch.6] as

$$\tilde{f}(x_k, \eta_{x_k}) = f(x_k) + \langle \text{grad } f(x_k), \eta_{x_k} \rangle + \frac{1}{2} \langle \text{Hess } f(x_k)[\eta_{x_k}], \eta_{x_k} \rangle, \quad (4.1)$$

where the Riemannian connection ∇ is used in the computation of the Hessian.

The stationary point of the local quadratic model is given by the Geometric Newton Equation

$$\text{Hess } f(x_k)[\eta_{x_k}] = -\text{grad } f(x_k), \quad \eta_{x_k} \in T_{x_k}\mathcal{M} \quad (4.2)$$

that provides a descent direction η_{x_k} for the real valued function h . Note that the equation lives in the tangent space at the current iterate. Once the descent direction has been computed solving (4.2), a *retraction* [13, Ch.4], i.e. a map $R_{x_k} : T_{x_k}\mathcal{M} \mapsto \mathcal{M}$ is needed to compute the next iterate. A typical retraction map is the exponential map associated to the Riemannian connection of \mathcal{M} . When computing the exponential map is expensive, a suitable approximation of the exponential map (that agrees up to the second derivative at the origin) can still be used, retaining the second order convergence rate.

The basin of attraction of the (geometric) Newton algorithm can be increased by employing a line search method to adjust the step length t_k in the optimal descent direction η_{x_k} . Since we are searching for stationary points, the function $h = \|\text{grad } f\|^2$ will be minimized along the search direction. In this paper, we make use of the **classical** Armijo's backtracking line search method [23]. Once the search direction and the step size have been found, the next it-

erate is computed and the procedure is repeated until the function h evaluated at the current iterate is sufficiently small.

The geometric Newton algorithm with line search can be summarized as follows

Algorithm 1 *Geometric Newton's Algorithm with line search.*

Input: $x_0 \in \mathcal{M}$, real valued function f on \mathcal{M} *Output:* Sequence of iterates x_1, \dots, x_n

1. *Search Direction:* solve (4.2) in η_{x_k} .
 2. *Step Size:* find $t_k = \arg \min_{\lambda} h(R_x(\lambda \eta_{x_k}))$
 3. *Update:* Set $x_{k+1} = R_x(t_k \eta_{x_k})$
-

In the following we will describe in detail the various steps required to solve (4.2). In particular, we will make use of the fact that as a manifold \mathcal{M} is embedded in the Euclidean Space \mathcal{E} , we can represent both points in \mathcal{M} and vectors in $T_x \mathcal{M}$ as elements of $\mathcal{E} \simeq T_x \mathcal{E}$, and use the Riemannian connection of \mathcal{E} to compute covariant derivatives on \mathcal{M} .

4.1 Geometric Newton Equation

Let \mathcal{M} denote a manifold endowed with a Riemannian metric $\langle \cdot, \cdot \rangle_{\mathcal{M}}$. Given a point $x \in \mathcal{M}$, and a function $f \in \mathfrak{F}(\mathcal{M})$, the Newton equation update for f at x is a system of equations linear in the argument η_x , ~~as $\text{Hess } f(x)[\eta_x]$ is a linear operator in the argument η_x .~~

The Riemannian gradient and Hessian are defined by

$$\begin{cases} \langle \text{grad } f(x), \xi_x \rangle_{\mathcal{M}} &= Df(x)[\xi_x] \\ \text{Hess } f(x)[\eta_x] &= (\nabla_{\eta_x} \text{grad } f)_x \end{cases}, \quad (4.3)$$

$\forall x \in \mathcal{M}$, and they can be evaluated exploiting the geometry of the ambient space \mathcal{E} . The approach described in [13, Ch.3] shows how to compute a representation of vectors in $T_x\mathcal{M}$ by means of the orthogonal projection of vectors in $T_x\mathcal{E}$. ~~This representation is handy since elements in $T_x\mathcal{E}$ can be represented in the same way of elements of \mathcal{E} itself, therefore~~ In this way, since $T_x\mathcal{E} \equiv \mathcal{E}$ and $T_x\mathcal{M} \subset T_x\mathcal{E}$, the same representation in \mathcal{E} can be used for elements in \mathcal{M} , $T_x\mathcal{M}$ and $T_x\mathcal{E}$. Moreover, in [Ref.](#) [13, ChS.3-5] it is shown how to compute the Riemannian gradient and Hessian of f , ~~and thus exploit second order information on the function f defined on \mathcal{M} , by means in terms~~ of the orthogonal projections of the gradient and Hessian of \bar{f} , where \bar{f} is any smooth extension of f in $\mathcal{E} \supseteq \mathcal{M}$. The gradient and Hessian of \bar{f} in \mathcal{E} , denoted by $\partial\bar{f}$ and $\partial^2\bar{f}[\eta]$ respectively, are called Euclidean gradient and Hessian.

4.2 Tangent Space Projection

To derive $\text{grad } f$ and $\text{Hess } f$, starting from the corresponding operators in \mathcal{E} , we use the projection tool developed in [ref.](#) [13].

The orthogonal projection operator

$$P_x : T_x\mathcal{E} \rightarrow T_x\mathcal{M} \quad (4.4)$$

$$\xi_x \mapsto P_x(\xi_x)$$

maps every tangent vector ξ_x of $T_x\mathcal{E}$ into its orthogonal projection onto $T_x\mathcal{M}$. In addition, every tangent vector ξ_x in $T_x\mathcal{E}$ admits the unique decomposition $\xi_x = \eta_x + \nu_x$, where $\eta_x \in T_x\mathcal{M}$ and $\nu_x \in \mathcal{M}^\perp$ (the normal space of \mathcal{M} at x , i.e. the orthogonal complement of $T_x\mathcal{M}$ to $T_x\mathcal{E}$). We have $\eta_x = P_x(\xi_x)$ and $\nu_x = \xi_x - P_x(\xi_x)$.

4.3 Riemannian Gradient

The connection between the Riemannian gradient $\text{grad } f$ of a function f from \mathcal{M} to \mathbb{R} , and $\partial\bar{f}$, the Euclidean gradient of a local smooth extension \bar{f} of f into \mathcal{E} is given by

$$\forall x \in \mathcal{M}, \text{grad } f(\bar{x}) = P_x(\partial\bar{f}(\bar{x})) \quad , \quad (4.5)$$

~~\bar{x} here denotes the canonical immersion of $x \in \mathcal{M}$ into \mathcal{E} [13].~~ we observe that x and \bar{x} represent the same point, regarded both as a point in \mathcal{M} and in \mathcal{E} .

4.4 Riemannian Hessian

In analogy with the Riemannian gradient, the Riemannian Hessian $\text{Hess } f$ of f at x , can be computed as the orthogonal projection onto $T_x\mathcal{M}$ of the tangent map of the extension to \mathcal{E} of the vector field $\text{grad } f$. Denoting with

$$D \text{grad } \bar{f}(x) : T_x\mathcal{E} \mapsto T_x\mathcal{E} \quad (4.6)$$

the directional derivative in \mathcal{E} of $\text{grad } f$ along η regarded as a vector field on \mathcal{E} , we have

$$\forall x \in \mathcal{M}, \text{Hess } f(x)[\eta] = P_x (D \text{grad } \bar{f}(x)[\eta]) . \quad (4.7)$$

We stress that in general $D \text{grad } \bar{f}(x) \neq D \partial \bar{f}(x) = \partial^2 \bar{f}(x)$, where $\partial^2 \bar{f}$ is the Euclidean Hessian of the extension \bar{f} of f [13, Ch.5]. At this point we can employ the projection operator P_x to compute $\text{grad } f$ and $\text{Hess } f$ as functions of $\partial \bar{f}$, $\partial^2 \bar{f}$, $D \text{grad } \bar{f}$ and x . It is not straightforward to give a general expression for $D \text{grad } \bar{f}$ from (4.5), and usually this relation is expressed in terms of the Weingardten map, also known as shape operator[21]. For the applications, we are considering it suffices to have a specific expression of $D \text{grad } \bar{f}(x)$ for the Oblique Manifold $\mathcal{OB}(2, N)$. **Convergence of Algorithm 1 can be pursued by a simple adaption of a result in [13, Chap. 4] and is lately described in the Appendix.**

5 The Newton's Algorithm on $\mathcal{OB}(2, N)$

A point $X \in \mathcal{OB}(2, N)$ and tangent vectors ξ_X, η_X to X can be represented by using $3 \times N$ dimensional matrices, i.e. as points and tangent vectors of the ambient space $\mathbb{R}^{3 \times N}$. Therefore, the orthogonal projection $P_X(\xi_X)$ of $\xi_X \in T_X \mathbb{R}^{3 \times N}$ and the directional derivative $D \text{grad } \bar{f}(X)$ can be represented by using $3 \times N$ dimensional matrices, as shown in Table 1. **Further details and the derivation of these expressions are given[22]. See [22] for further details. In**

the following subsections we detail the main steps of the Newton's Algorithm on $\mathcal{OB}(2, N)$.

\mathcal{M}	$\mathcal{OB}(2, N)$
x	X
$P_x(\xi_x)$	$P_X(\xi_X) := \xi_X - d(X^T \xi_X) X$
$D \text{grad } \bar{f}(x)[\eta_x]$	$D \text{grad } \bar{f}(X)[\eta_X] = P_X(\partial^2 \bar{f}(X)[\eta_X]) - d(X^T \partial \bar{f}(X)) \eta_X$

Table 1 Expression for the coordinate representation of $D \text{grad } \bar{f}(x)[\eta_x]$ and of $P_x(\xi_x)$ on the Oblique manifold $\mathcal{OB}(2, N)$.

5.1 Solution to the Newton equation

Recalling that the Newton update (4.2) is a system of linear equations with solution set belonging to $T_X \mathcal{OB}(2, N)$, which is a subspace of $T_X \mathbb{R}^{3 \times N}$, one basis of $T_X \mathcal{OB}$ for computing the solution can be built by means of a nonlinear function of X , exploiting the geometric structure $\mathcal{OB}(2, N)$, seen as the Cartesian product of N unit spheres. We denote with $\text{grad } f_k(X)$ and X_k the N columns of the matrices $\text{grad } f(X)$ and X , and with \mathbf{e}_k the canonical basis row vectors of \mathbb{R}^N . We also consider the map $\text{vect}(\cdot)$ that vectorize the matrix $\xi_X \in \mathbb{R}^{3 \times N}$ into a $3N$ dimensional column vector $\text{vect } \xi_X$. **Nella seguente proposizione, proposta di definire prima gli oggetti e poi 5.2 e 5.3**

Proposition 5.1 *Let $X \in \mathcal{OB}(2, N)$ and $f : M \mapsto \mathbb{R}$ such that $\text{grad } f_k(X) \neq \mathbf{0}$, $k = 1, \dots, N$. Then (4.2) for f and x is equivalent to*

$$H(X)\mathbf{y} = \mathbf{g}(X), \mathbf{y} \in \mathbb{R}^{2N} \quad (5.1)$$

where

$$\begin{pmatrix} \mathbf{g}(X) \\ 0_{N \times 1} \end{pmatrix} = T(X) \text{vect grad } f(X), \quad (5.2)$$

$$T(X) = (\text{vect } \mathbf{v}_1, \dots, \text{vect } \mathbf{v}_N, \text{vect } \mathbf{w}_1, \dots, \text{vect } \mathbf{w}_N, \text{vect } \mathbf{q}_1, \dots, \text{vect } \mathbf{q}_N)^T, \quad (5.3)$$

$H(X)$ is the principal minor of $T(X)\tilde{H}(X)T(X)^T$ with indexes ranging from 1 to $2N$, $\tilde{H}_{ik}(X) = \langle \mathbf{e}_i, \text{Hess } f(X)[\mathbf{e}_k] \rangle$. Here $\mathbf{v}_k = \text{grad } f_k(X) \otimes \mathbf{e}_k$, $\mathbf{w}_k = (\text{grad } f_k(X) \wedge X_k) \otimes \mathbf{e}_k$, $\mathbf{q}_k = X_k \otimes \mathbf{e}_k$, and \mathbf{e}_k are the canonical basis vectors of \mathbb{R}^N .

The proof of Proposition 5.1 can be found in the Appendix. We observe that, if $\text{grad } f_k(X) = \mathbf{0}$ for some k , the k -th column of the vector η_X representing the solution can be taken equal to the null vector of \mathbb{R}^3 , and one can rearrange the basis vectors avoiding to account for this three components in the linear equation system (4.2).

5.2 Retraction for $\mathcal{OB}(2 \times N)$

Despite the fact that each Riemannian manifold has a natural retraction in the exponential map, different retractions are usually employed to minimize computational costs. For $\mathcal{OB}(2, N)$, the map

$$R(X, \xi_X) = (X + \xi_X) d((X + \xi_X)^T (X + \xi_X))^{-1/2}, \quad (5.4)$$

i.e., the normalization to unit norm of each column of the matrix $X + \xi_X$, is a retraction for $\mathcal{OB}(2, N)$ [13, 21, 22].

5.3 Armijo Backtracking Line Search

An effective and computationally efficient line search algorithm is the Armijo Algorithm[24], [13, Ch.4]. At each iterate, the step size t_k is set to $\alpha\beta^l$, with l the smallest integer such that **La formula seguente stata rimaneggiata per mettere in evidenza h e m_h**

$$h(R(t_k\eta_x)) \leq h(x) + \sigma\gamma_k Dh(x)[\eta_x] , \quad (5.5)$$

for a sufficiently small parameter σ , with x denoting the current iterate and η_x the current descent direction. Here $\alpha > 0$, and $\beta, \sigma \in (0, 1)$ are design parameters. Condition (5.5) assure the convergence of the line search if the function $h(R(t_k\eta_x))$ to be minimized is sufficiently smooth (continuously differentiable with Lipschitz derivative).

5.4 Discussion and Convergence

questa sezione stata spostata nell'appendice.

6 Application to Square Ring Laser Cavity

Consider now the case of an optical cavity made by $N = 4$ spherical mirrors whose centers approximately lie on a planar square. The motivation for ana-

lyzing such configuration is the design of control algorithms for the GINGER array of ring lasers [8]. With four mirrors, $\mathcal{E} = \mathbb{R}^{3 \times 4}$ and $\mathcal{M} = \mathcal{OB}(2, 4)$.

The configuration and parameters of the optical cavity are

$$X = (\mathbf{x}_1, \dots, \mathbf{x}_4) \in \mathcal{OB}(2, 4), \quad (6.1)$$

$$C = (\mathbf{c}_1, \dots, \mathbf{c}_4) \in \mathbb{R}^{3 \times 4}, \quad (6.2)$$

and

$$Q = \text{diag}(r_1, r_2, r_3, r_4) \in \mathbb{R}^{4 \times 4}; \quad (6.3)$$

In matrix form, the coordinates of the light spots on the mirror surface are given by

$$Z = XQ + C, \quad (6.4)$$

where the matrix $Z = (\mathbf{z}_1, \mathbf{z}_2, \mathbf{z}_3, \mathbf{z}_4)$.

The 4 vectors that describe the sides of the polygonal cavity, i.e., the vectors joining the spots on consecutive mirror surfaces (see Fig.7.3), are given by $\mathbf{y}_k = (\mathbf{z}_{k+1} - \mathbf{z}_k)$, $k = \{1, 2, 3, 4\}$ with $\mathbf{z}_5 := \mathbf{z}_1$. The length of the optical path, the vector area and compactness ratio are $p(X; C, Q) = \sum_{i=1}^4 \|\mathbf{y}_i\|$, $\mathbf{a}(X; C, Q) = \frac{1}{2} \sum_{k=1}^{N-1} \mathbf{z}_k \wedge \mathbf{z}_{k+1}$, and $\mathbf{k}_r(X; C, Q) = \mathbf{a}(X; C, Q)/p(X; C, Q)$,

respectively. Defining

$$Y = ZM, \quad M = \begin{pmatrix} 1 & 0 & 0 & -1 \\ -1 & 1 & 0 & 0 \\ 0 & -1 & 1 & 0 \\ 0 & 0 & -1 & 1 \end{pmatrix},$$

the optical path length can be written as

$$p(X; C, Q) = \text{tr} \left(d(Y^Q Y)^{1/2} \right), \quad (6.5)$$

Note that the square root operator $(\cdot)^{1/2}$ acts component wise on the entries of the diagonal matrix $d(W)$.

Let \bar{p} denote the extension of the function p to \mathcal{E} . Using (6.4) and (6.5) the Euclidean gradient and Hessian of \bar{p} are given by

$$\langle \partial \bar{p}(X), \xi \rangle = \text{tr} \left[d(Y^T Y)^{-1/2} d(Y^T \xi_X Q M) \right], \quad (6.6)$$

and

$$\langle \partial^2 \bar{p}(X)[\eta], \xi \rangle = \text{tr} \left[d(Y^T Y)^{-1/2} d(M^T Q \xi_X^T \eta_X Q M) \right] \quad (6.7)$$

$$- \text{tr} \left[d(Y^T Y)^{-3/2} d(Y^T \eta_X Q M) d(Y^T \xi_X Q M) \right], \quad (6.8)$$

respectively. The Riemannian gradient and Hessian of p can be calculated from (6.6) and (6.7) with the help of (4.5) and (4.7).

Let us consider a square optical cavity of side L and four mirrors with the same curvature radius, i.e.

$$C^* = \left(r - \frac{L}{\sqrt{2}}\right) \begin{pmatrix} 1 & 0 & -1 & 0 \\ 0 & 1 & 0 & -1 \\ 0 & 0 & 0 & 0 \end{pmatrix}, \quad (6.9)$$

$$Q^* = \text{diag}(r, r, r, r),$$

so that $p(X^*; C^*, Q^*) = 4L$. The point $X^* = -(r - L/\sqrt{2})^{-1}C^*$ lays in $\mathcal{OB}(2, 4)$, and one can check that X^* is an extremum of p using (6.6), (6.7), and the formulas of Table 1. The eigenvalues of $\text{Hess } p$ at the point X^* are

$$\Sigma(\text{Hess } p(X^*)) = -\sqrt{2} r \left(1, 1, 1 - \frac{L}{\sqrt{2}r}, 1 - \frac{L}{\sqrt{2}r}, 1 - \frac{\sqrt{2}L}{r}, 1 - \frac{\sqrt{2}L}{r}, 1 - \frac{\sqrt{2}L}{r}, 1 - \frac{4L}{\sqrt{2}r} \right). \quad (6.10)$$

All the eigenvalues of $\text{Hess } p$ are non-zero provided that the ration L/r is not equal to $\sqrt{2}$, $1/\sqrt{2}$, or $\sqrt{2}/4$ which correspond to unstable optical cavity configurations [7]. For a stable optical cavity the Riemannian Hessian has non-zero eigenvalues, therefore X^* is an isolated root of $\text{grad } p$ and a saddle point of p , as the spectrum of the Hessian (6.11) has both strictly positive and negative eigenvalues. If a stable optical cavity is slightly misaligned from C^* , by the continuity of p , the Riemannian gradient will have isolated roots, and so the eigenvalues of the Riemannian Hessian will be different from zero and the Newton algorithm will converge to the path which satisfies the Fermat's principle.

7 Numerical Study

The proposed geometric Newton algorithm has been tested by Monte Carlo techniques. Optical cavity configurations are generated starting with mirror positions close to square configuration C^* , with $L= 1.6$ m and represented by 3×4 random matrices whose entries are uniformly distributed over the set $\{|C_{ij} - C_{ij}^*| < \sigma\}$, with σ ranging from $10^{-6}L$ to $10^{-2}L$ with a logarithmic spaced step of $L/10$. The radii matrix used is $Q = rI_{4 \times 4}$, with $r = 4$ m. The chosen values correspond to the design of GP2 ring laser [7]. The geometric Newton algorithm has been applied to find the saddle point of the function p , starting from the trial configuration X^* . This procedure has been repeated 10^4 times to assess whether mirror displacements are small enough for satisfying the convergence properties of the algorithm. All the runs do not show ill-conditioning problems in the Newton vector computation. In addition, the algorithm took at most 3 iterations to generate an iterate such that $\|\text{grad } p(x)\| < 10^{-12}$ m; quadratic convergence is also attained, as expected since the problem satisfies second order sufficient condition for optimality (i.e., positive definiteness of the Hessian at the optimal point). In all the Monte Carlo runs the computed laser spots positions are saddle points of p . To better illustrate how the algorithm works, we show in Figure 7.1 the typical behavior of $\|\text{grad } p(x)\|$ in a run with $\sigma \sim 0.5$ m. The algorithm took 5 iterations to converge. In Figure 7.2 two comparisons are displayed, between the function p and its second order geometric model, and between the function h and the Armijo condition for h , respectively.

In the figure $m_f(\lambda) = f(x_k) + \langle \text{grad } f(x_k), \lambda \eta_x \rangle + 1/2 \langle \text{Hess } f(x_k)[\lambda \eta_x], \lambda \eta_x \rangle$, $m_h(\lambda) = h(x) + \sigma \langle \text{grad } h(x_k), \lambda \eta_x \rangle$, $\lambda \in [0, 1]$, $\sigma = 1/2$ and $\eta_x = \eta_{x_k}$ is the Newton vector at the iteration k . Each of the 5 iterations of the run reported in Figure 7.1 is displayed. We note that the optical path length p is well modeled by the second order geometric model starting from the first iteration, and that condition (5.5) allows for step sizes t_k closer to the unity, like in pure Newton methods, as the iteration number increase.

In Figure 7.3 we draw an illustrative example of mirror displacements and the corresponding laser beams as calculated by Fermat's principle.

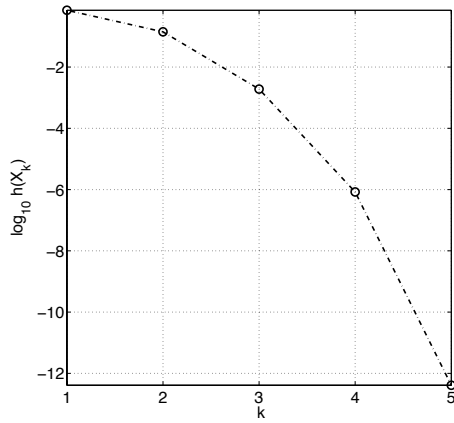


Fig. 7.1 Plot of $h(x_k) = \|\nabla p(x_k)\|$ versus the iteration index k .

8 Conclusions

We have adressed the problem of computing the light path in optical cavities as a function of the mirror positions and orientations by means of the Fermat's principle. To find the stationary optical path in a polygonal cavity, a geometric

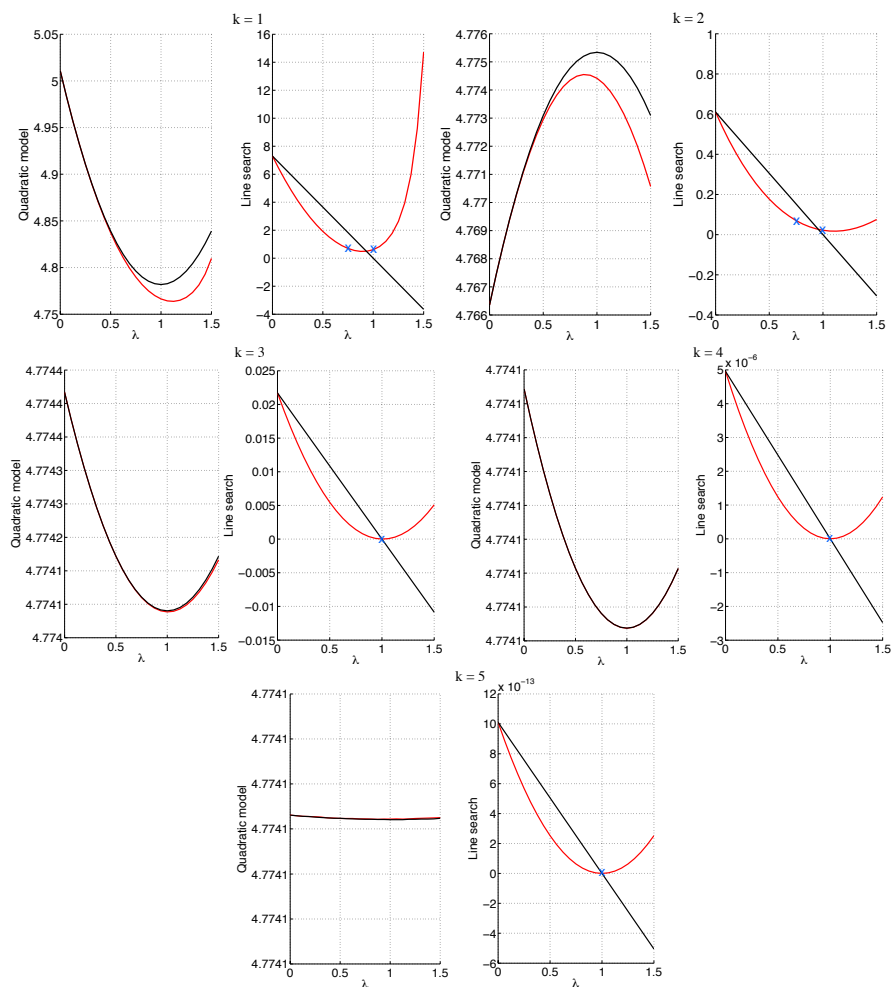


Fig. 7.2 Left plots: Comparison between the functions p (red lines) and its second order geometric model m_f (black lines). Right plots: Comparison between the function h (red lines) and m_h , related to the Armijo condition on h (black lines). The blue crosses represent the iterates of the line search method. The plots are relative to consecutive algorithm iterations from 1 to 5.

Newton method is proposed, exploiting the embedding of the Oblique Manifold $\mathcal{OB}(2, N)$ in the Euclidean space $\mathbb{R}^{3 \times N}$ for the computation of Riemannian gradient and Hessian of the optical path length. The Riemannian gradient and

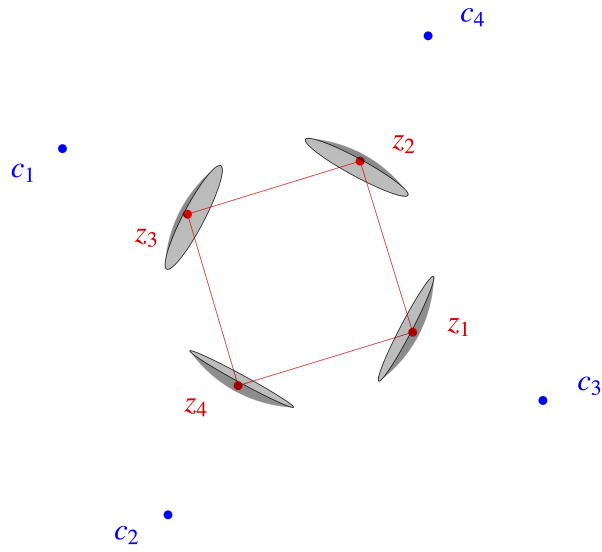


Fig. 7.3 An example of displacements of mirrors forming a square optical cavity. Elements relative to each mirror are colored in grey. Red dots mark the mirror centers, the red lines represent the optical path length as a link between consecutive laser spots z_k .

Hessian are then used in each step of the Newton iteration. The algorithm exhibits second order convergence rate. ~~Our approach is motivated by the need to compute the optical path of the laser beams in resonant cavities, and our results allow for the application of control techniques to constrain the beams path. With the help of the results obtained in [13], we proved the correctness and quadratic convergence rate of our algorithm~~ under mild assumptions of regularity of the function p . Using smoothness we showed that the function p meets the regularity requirements in a neighborhood of the point C^* , representing the perfectly aligned squared cavity. Monte Carlo simulations have shown that this neighborhood contains all the cavity configurations that can be encountered in practice for heterolithic ring lasers. In fact, manufacture

tolerances of a ring laser frame ensure $\|C - C^*\| \sim 10^{-5} L$, while we showed that our algorithm successfully evaluates the beam steering of a square cavity with errors in mirror positioning or alignment up to $10^{-3}L$. The geometric Newton method we devised provides a relative accuracy of 1 part in 10^{12} in evaluating the optical cavity configuration of a square ring laser. It is worth noticing that greater precisions can be achieved, even if they are not of physical interest. The computational cost of the proposed method is very low, since at most 3 iterations are required to reach the desired accuracy in the Riemannian gradient norm in Monte Carlo simulations. ~~The treatment of an optical cavity in the framework of differential geometry is more suitable for an extension of geometrical optics formalism which includes also the description of Gaussian beams. The geometric approach described in the present paper seems to be well suited to deal with geometrical optics problems where Gaussian profiles are used for beam description. However, much work has still to be devoted to a suitable description of the cavity configurations, and to a dynamical model for an active control of the laser optical path in resonant cavities. Such further investigations will allow us to estimate the sensitivity and long term stability of heterolithic ring lasers, with the aim to highlight their promising applications to the fundamental physics, e.g. General Relativity or Axion detection[5]. Once the laser beam configuration in the cavity is determined by Fermat's principle, the calibration and active control of the optical cavity can be formulated as a optimization problem. The problem of the absolute calibration and control of a ring laser cavity would deserve further investigation and it will be the~~

~~topic of a forthcoming paper [25].~~ Based on the presented algorithm, future work will be devoted to the calibration and active control of resonant optical cavities [25].

References

1. K.U. Schreiber and J-P. R. Wells, Large ring lasers for rotation sensing, *Rev. Sci. Instrum.* 84, 4, 041101, (2013).
2. D. Cuccato, et al. Controlling the non-linear intracavity dynamics of large He- Ne laser gyroscopes, *Metrologia*, 51, 1, 97, (2014).
3. A. Beghi, et al. Compensation of the laser parameter fluctuations in large ring-laser gyros: a Kalman filter approach, *Appl. Opt.* 51, 7518-7528, (2012).
4. K. U. Schreiber, A. Gebauer, and J.-P. R. Wells, Long-term frequency stabilization of a 16 m^2 ring laser gyroscope, *Opt. Lett.* 37, 1925-1927 (2012).
5. F. Bosi, et al. Measuring gravitomagnetic effects by a multi-ring-laser gyroscope, *Phys. Rev. D*, 84, 12, 122002, (2011).
6. A. Di Virgilio et al. Performances of G-Pisa: a middle size gyrolaser, *Classical and Quantum Gravity*, 27, 8, 084033, (2010).
7. R. Santagata et al. Optimization of the geometrical stability in square ring laser gyroscopes, *Classical and Quantum Gravity*, 32, 5, 055013, (2015).
8. J. Belfi et. al. Interferometric length metrology for the dimensional control of ultra-stable ring laser gyroscopes, *Classical and Quantum Gravity*, 31, 22, 225003 (2014).
9. A. Di Virgilio et al. A ring lasers array for fundamental physics, *C. R. Physique*, 15, 10, 866-874 (2014).
10. For the Romy project see: <http://www.geophysik.uni-muenchen.de/ROMY/>.
11. Y. J. L. Xingwu and C. Meixiong, Generalized ray matrices for spherical mirror reflection, *Optics Express* 19, 7, 6762-76, (2011).
12. B. E. A. Saleh and M. Carl, *Resonator Optics*, John Wiley & Sons, Inc. Teich (2001).

13. P.-A. Absil, R. Mahony and R. Sepulchre, Optimization Algorithms on Matrix Manifolds, Princeton University Press, (2008).
14. J. E. Marsden and T. Ratiu, Manifolds, Tensor Analysis, and Applications, Springer, (2002).
15. Ghatak, Ajoy (2009), Optics (4th ed.), ISBN 0-07-338048-2.
16. M. Ishteva, et. al., Differential-geometric Newton method for the best rank- (R_1, R_2, R_3) approximation of tensors, Numerical Algorithms, 51, 2, 179-194 (2009).
17. M. Kallay, A geometric Newton-Raphson strategy, Computer Aided Geometric Design, 18, 8, 797-803 (2001).
18. L. De Lathauwer, B. De Moor, and J. Vandewalle, On the best rank-1 and rank- (r_1, r_2, \dots, r_n) approximation of higher-order tensors, SIAM. J. Matrix Anal. & Appl., 21(4), 1324-1342 (2000).
19. S. Amat, S. Busquiera and J.M. Gutierrez, Geometric constructions of iterative functions to solve nonlinear equations, Journal of Computational and Applied Mathematics, 157, 1, 197-205 (2003).
20. P.-A. Absil, M. Ishteva and L. De Lathauwer, A Geometric Newton Method for Oja's Vector Field, MIT press journal on Neural Computation, 21, 5, 1415-1433 (2009).
21. P.-A. Absil, R. Mahony, J. Trumpf, An Extrinsic Look at the Riemannian Hessian, Geometric Science of Information, 8085, 361-368, (2013).
22. N. Boumal et al. Manopt, a Matlab toolbox for optimization on manifolds, The Journal of Machine Learning Research, 15, 1, 1455-1459 (2014).
23. L. Armijo, Minimization of functions having Lipschitz continuous first partial derivatives, Pacific Journal of Mathematics 16, 1, 1-3 (1966).
24. Nocedal, Wright, Numerical Optimization, 2006, ISBN:978-0-387-30303-1.
25. A. Beghi, D. Cuccato, A. Ortolan, A. Saccon, Shape and pose of four points in \mathbb{R}^3 (in preparation).

A Discussion and Convergence of Algorithm 1

questa sezione stata spostata nell'appendice. In Algorithm 1 at each iteration the Newton equation (4.2) is solved for the function f , then the function $h(x) = \|\text{grad } f(x)\|^2$ is minimized along the computed direction. In this way we need to compute only $\text{Hess } f$ and $\text{grad } f$, avoiding the computation of $\text{Hess } h$, that would require to compute the third derivative of f .

Proposition A.1 *Algorithm 1 converges to the stationary point x^* of the function f with quadratic convergence rate, provided that, in a neighborhood $\mathcal{I}(x^*)$ of x^* , $\text{grad } f \neq 0$, $\text{Hess } f$ is injective, and the first iterate is $x_0 \in \mathcal{I}(x^*)$.*

Proof Let x denote a generic algorithm iterate, By hypotheses the Newton vector η_x , solution of (4.2), is well defined. The Riemannian gradient of h reads

$$\text{grad } h = 2\text{Hess } f[\text{grad } f] . \quad (\text{A.1})$$

By evaluating the expression $Dh(x)[\eta_x]$ we get

$$\begin{aligned} Dh(x)[\eta_x] &= 2 \langle \text{grad } f(x), \text{Hess } f(x)[\text{Hess } f(x)^{-1}[-\text{grad } f(x)]] \rangle & (\text{A.2}) \\ &= -2 \|\text{grad } f(x)\|^2 \\ &= -2h(x). \end{aligned}$$

The sequence $\{\eta_{x_k}\}$ is gradient related to $\{x_k\}$. In fact by hypothesis and (A.1) it holds $\text{grad } h(x_k) \neq 0$, therefore, using (A.2) we get $-2 \sup_{\mathcal{I}(x^*)} h(x_k) = \sup_{\mathcal{I}(x^*)} Dh(x_k)[\eta_{x_k}] < 0$. By the smoothness of the functional $\text{Hess } f$ and of the vector field $\text{grad } f$, since $\mathcal{I}(x^*)$ is a compact set, we can conclude that $\{\eta_{x_k}\}$ is bounded. Hence Algorithm 1 fits in the framework of Theorem 4.3.1 and Theorem 6.3.2 [13, Chs.4-6], stating that every accumulation point of $\{x_k\}$ is a critical point of h , so that the local quadratic convergence holds. \square

Note that the Armijo condition (5.5) for the function h and the direction η_x can be rewritten as

$$h(x) - h(y_k) < -\sigma\gamma_k Dh(x)[\eta_x] = 2\sigma\gamma_k h(x) \quad (\text{A.3})$$

$$h(y_k) > (1 - 2\sigma\gamma_k) h(x) , \quad (\text{A.4})$$

where $y_k = R_x(\gamma_k \eta_x)$, $x = x_k$, $\eta_x = \eta_{x_k}$, and k is the iteration number.

B Proof of Proposition 5.1

Proof We recall that \mathbf{e}_k are the canonical basis vectors of \mathbb{R}^N . Suppose that $\text{grad } f_k(X) \neq \mathbf{0}$ for $k = 1, \dots, N$. Each X_k is orthogonal to the corresponding $\text{grad } f_k(X)$ by the definition of $T_X \mathcal{OB}(2, N)$ since $X_k \neq \mathbf{0}$ and $\text{grad } f_k(X) \neq \mathbf{0}$. Therefore the vectors $\mathbf{v}_k = \text{grad } f_k(X) \otimes \mathbf{e}_k$ and $\mathbf{w}_k = (\text{grad } f_k(X) \wedge X_k) \otimes \mathbf{e}_k$ are mutually orthogonal, and they belong to $T_x \mathcal{OB}(2, N)$ by construction, therefore the set $\{\mathbf{v}_1, \dots, \mathbf{v}_N, \mathbf{w}_1, \dots, \mathbf{w}_N\}$ is a basis of $T_X \mathcal{OB}(2, N)$. The vectors $\mathbf{q}_k = X_k \otimes \mathbf{e}_k$, are mutually orthogonal and belong to the normal space of $T_X \mathcal{OB}(2, N)$; therefore $(\mathbf{v}_1, \dots, \mathbf{v}_N, \mathbf{w}_1, \dots, \mathbf{w}_N, \mathbf{q}_1, \dots, \mathbf{q}_N)$ is a suitable basis of $T_x \mathbb{R}^{3 \times N}$ and

$$T(X) = (\text{vect } \mathbf{v}_1, \dots, \text{vect } \mathbf{v}_N, \text{vect } \mathbf{w}_1, \dots, \text{vect } \mathbf{w}_N, \text{vect } \mathbf{q}_1, \dots, \text{vect } \mathbf{q}_N)^T \quad (\text{B.1})$$

is the basis change matrix associated.

To prove the proposition we recast (4.2) in a suitable form. We get

$$T(X) \text{vect } \eta_X = \begin{pmatrix} \mathbf{y}(X) \\ 0 \end{pmatrix}, \quad T(X) \mathbf{z}(X) = \begin{pmatrix} \mathbf{g}(X) \\ 0 \end{pmatrix}, \quad (\text{B.2})$$

Defining the matrix $\tilde{H}(X) \in \mathbb{R}^{12 \times 12}$, where $\tilde{H}_{ik}(X) = \langle \mathbf{e}_i, \text{Hess } f(X)[\mathbf{e}_k] \rangle$, the Newton Equation (4.2) can be rewritten as

$$H(X) \mathbf{y}(X) = \mathbf{g}(X) , \quad (\text{B.3})$$

where $\mathbf{y}(X) \in \mathbb{R}^{2N}$ and $H(X)$ is the principal minor of $T(X) \tilde{H}(X) T(X)^T$ with indexes ranging from 1 to $2N$.

If the Matrix $H(X)$ is not singular, an expression for the Newton vector at each iteration is therefore: $\text{vect } \eta_X = T(X)^T (H(X)^{-1} \mathbf{g}(X), 0)^T$. \square